$X(3872)$ to $\psi(2S)$ yield ratio in heavy-ion collisions

L. M. Abreu,[1,2,*] F. S. Navarra,[2,†] and H. P. L. Vieira[1,‡]

[1]*Instituto de Física, Universidade Federal da Bahia, Campus Universitário de Ondina, 40170-115, Bahia, Brazil*

[2]*Instituto de Física, Universidade de São Paulo, Rua do Matão, 1371, CEP 05508-090, São Paulo, SP, Brazil*

(Received 29 January 2024; accepted 2 June 2024; published 9 July 2024)

In this work, we evaluate the $X(3872)$ to $\psi(2S)$ yield ratio ($N_X/N_{\psi(2S)}$) in Pb-Pb collisions, taking into account the interactions of the $\psi(2S)$ and $X(3872)$ states with light mesons in the hadron gas formed at the late stages of these collisions. We employ an effective Lagrangian approach to estimate the thermally averaged cross sections for the production and absorption of the $\psi(2S)$ and use them in the rate equation to determine the time evolution of $N_{\psi(2S)}$. The multiplicity of these states at the end of the mixed phase is obtained from the coalescence model. The multiplicity of $X(3872)$, treated as a bound state of $(D\bar{D}^* + \mathrm{cc})$ and also as a compact tetraquark, was already calculated in previous works. Knowing these yields, we derive predictions for the ratio ($N_X/N_{\psi(2S)}$) as a function of the centrality, of the center-of-mass energy, and of the charged hadron multiplicity measured at midrapidity $[dN_{ch}/d\eta(\eta < 0.5)]$. Finally, we make predictions for this ratio in Pb-Pb collisions at $\sqrt{s_{NN}} = 5.02$ TeV to be measured by the ALICE Collaboration in run 3. Our findings suggest that the molecular configuration generates a ratio compatible with the data, whereas the ratio obtained with the tetraquark configuration is 50 times smaller.

DOI: 10.1103/PhysRevD.110.014011

I. INTRODUCTION

Among the new hadrons observed in the past two decades [1], several have properties incompatible with the quark model predictions and can be classified as unconventional states. For recent reviews, see [2–4]. Their properties remain the subject of intense debate, and this makes exotic quarkonium spectroscopy a hot topic of research. The most relevant question is: Which is their structure? They can be weakly bound hadron molecules, compact multiquark states, cusps generated from kinematical singularities, excited conventional hadrons, glueballs, hybrids, etc., or even a superposition of different configurations. So far, there is no compelling answer to this question.

One emblematic example is the first-observed and most famous exotic state, $X(3872)$ [1,5]. Its intrinsic nature is still a matter of controversy. Two configurations are the most explored in the literature [2–4]: the shallow bound state of open charm mesons $(D\bar{D}^* + \mathrm{cc})$ and the $c\bar{c}q\bar{q}$ compact tetraquark. The ultimate goal of the present work is to contribute to the determination of the $X(3872)$ structure.

A new era in the investigation of exotic charmonium states has started with the first observation of $X(3872)$ in relativistic heavy-ion collisions reported recently by the CMS Collaboration [6]. The data were collected in lead-lead (Pb-Pb) collisions at a center-of-mass energy $\sqrt{s} = 5.02$ TeV per nucleon pair, using the decay chain $X(3872) \to J/\psi\pi^+\pi^- \to \mu^+\mu^-\pi^+\pi^-$. The rapidity and transverse momentum intervals considered were $|y| < 1.6$ and $15 < p_T < 50$ GeV, respectively. The significance of the inclusive $X(3872)$ signal was 4.2σ. Interestingly, the prompt $X(3872)$ to $\psi(2S)$ yield ratio was found to be

$$\mathcal{R} = \frac{N_{X(3872)}}{N_{\psi(2S)}} = 1.08 \pm 0.49(\mathrm{stat}) \pm 0.52(\mathrm{syst}). \quad (1)$$

This central value is about one order of magnitude higher than the one observed in pp collisions [7], which is close to 0.09. Additionally, the LHCb Collaboration reported the observation of $X(3872)$ in p-Pb collisions at both

*luciano.abreu@ufba.br
†navarra@if.usp.br
‡hildeson.paulo@ufba.br

forward and backward rapidity and at $\sqrt{s} = 8.16$ TeV per nucleon [8]. The decay chain was the same as the one studied by the CMS Collaboration. The transverse momentum interval considered was $p_T > 5$ GeV, and the rapidity intervals were $1.5 < y < 4$ for p-Pb (forward configuration) and $-5 < y < -2$ for Pb-p (backward configuration). The resulting ratios of the $X(3872)$ to $\psi(2S)$ multiplicities were $0.27 \pm 0.08 \pm 0.05$ in p-Pb and $0.36 \pm 0.15 \pm 0.11$ in Pb-p. Both are bigger than the one seen in pp collisions but smaller than the one observed in Pb-Pb collisions.

On the theoretical side, some recent works have attempted to describe the data. In Ref. [9], the coalescence model has been used to estimate N_X and the statistical hadronization model to obtain $N_{\Psi(2S)}$. The obtained ratio has a central value of 0.806 for $X(3872)$ in the molecular configuration and 0.204 for the tetraquark configuration. In Ref. [9], the interaction of X [and also of the $\psi(2S)$] with the light mesons in the hadron gas was not considered. Here, we try to estimate the effect of these interactions on the ratio $\mathcal{R}$.

At the beginning of a heavy-ion collision, quark-gluon plasma (QGP) is formed. It expands, cools down, and hadronizes into a hot hadron gas. The gas lives for about 10 fm and freezes out, generating the observed particles. Conventional and exotic hadrons formed in the end of the mixed phase can interact with the (mostly light) particles in the hadron gas, and their multiplicities may experience modifications due to production and absorption processes, as was pointed out in previous works [10–20]. The case of $X(3872)$ has been studied [10–12,16], and its final multiplicity will depend on the interaction cross sections, which, in turn, depend on the spatial configuration of the quarks. Meson molecules are larger and, therefore, have greater cross sections and stronger interaction with the hadronic medium than compact tetraquarks. In order to have a more complete description of the process, these interactions should be taken into account.

Motivated by these recent measurements in Pb-Pb and p-Pb collisions, in this work we evaluate the ratio $\mathcal{R}$ taking into account the interactions of the $\psi(2S)$ and of the $X(3872)$ states with the hadron gas formed in heavy-ion collisions. We will make use of effective Lagrangians to estimate the thermally averaged cross sections for $X(3872)$ and $\psi(2S)$ production and absorption and employ them in the rate equation to determine the time evolution of the ratio $\mathcal{R}$. We will use the coalescence model to compute the multiplicity of these states at the end of the mixed phase. $X(3872)$ will be treated as a bound state of $(D\bar{D}^* + \mathrm{cc})$ and also as a compact tetraquark. Finally, we will make predictions for $\mathcal{R}$ to be measured by the ALICE Collaboration in run 3. We emphasize that we will study only the interactions in the hadron gas phase which occur after the hadronization of the QGP and involve only hadronic degrees of freedom.

II. EFFECTIVE FORMALISM

In what follows, we describe the effective formalism used to evaluate the interactions of the $X(3872)$ and $\psi(2S)$ states with the surrounding hadronic medium. In particular, we consider the medium constituted of the lightest and most abundant pseudoscalar and vector mesons, i.e., the pions and ρ mesons, and take into account the lowest-order Born contributions. The reactions involving $X(3872)$ have already been studied in previous works, and for the sake of conciseness we will not reproduce them here. We refer the reader to Refs. [10–12,16] for a detailed discussion.

To the best of our knowledge, in contrast to the case of J/ψ [21–23], there is no effective theory for the reactions involving $\psi(2S)$. In the lack of works on this subject, we adopt an effective approach, based on the J/ψ studies, to describe the reactions $\psi(2S)\pi \to \bar{D}^{(*)}D^{(*)}$ and $\psi(2S)\rho \to \bar{D}^{(*)}D^{(*)}$, as well as the inverse processes. In Figs. 1 and 2, we show the lowest-order Born diagrams contributing to each process. To calculate their respective cross sections, we will adapt the effective Lagrangians introduced in [21–23]. The couplings involving the $\psi(2S)$ and the D^* mesons are [we denote $\psi(2S) \equiv \psi$]

$$\begin{aligned}
\mathcal{L}_{\psi DD} &= g_{\psi DD}\psi_\mu(\partial^\mu D\bar{D} - -D\partial^\mu\bar{D}),\\
\mathcal{L}_{\psi D^*D^*} &= -ig_{\psi D^*D^*}[\psi^\mu(\partial_\mu D^{*\nu}\bar{D}^*_\nu - -D^{*\nu}\partial_\mu\bar{D}^*_\nu)\\
&\quad + (\partial_\mu\psi_\nu D^{*\nu} - \psi_\mu\partial_\nu D^{*\nu})\bar{D}^{*\mu}\\
&\quad + D^{*\mu}(\psi^\nu\partial_\mu\bar{D}^*_\nu - \partial_\mu\psi_\nu\bar{D}^{*\nu})],\\
\mathcal{L}_{\psi DD^*} &= -g_{\psi DD^*}\epsilon^{\mu\nu\alpha\beta}\partial_\mu\psi_\nu(\partial_\alpha D^*_\beta\bar{D} + D\partial_\alpha\bar{D}^*_\beta);
\end{aligned} \tag{2}$$

while the vertices involving the D^* mesons and the pions and ρ mesons are

$$\begin{aligned}
\mathcal{L}_{\pi DD^*} &= ig_{\pi DD^*}D^{*\mu}\vec{\tau}\cdot(\bar{D}\partial_\mu\vec{\pi} - \partial_\mu\bar{D}\,\vec{\pi}) + \mathrm{H.c.},\\
\mathcal{L}_{\rho DD} &= ig_{\rho DD}(D\vec{\tau}\partial_\mu\bar{D} - \partial_\mu D\vec{\tau}\,\bar{D})\cdot\vec{\rho}^\mu,\\
\mathcal{L}_{\rho D^*D^*} &= ig_{\rho D^*D^*}[(\partial_\mu D^{*\nu}\vec{\tau}\bar{D}^*_\nu - D^{*\nu}\vec{\tau}\partial_\mu\bar{D}^*_\nu)\cdot\vec{\rho}^\mu\\
&\quad + (D^{*\nu}\vec{\tau}\cdot\partial_\mu\vec{\rho}_\nu - \partial_\mu D^{*\nu}\vec{\tau}\cdot\vec{\rho}_\nu)\bar{D}^{*\mu}\\
&\quad + D^{*\mu}(\vec{\tau}\cdot\vec{\rho}^\nu\partial_\mu\bar{D}^*_\nu - \vec{\tau}\cdot\partial_\mu\vec{\rho}^\nu\bar{D}^*_\nu)],\\
\mathcal{L}_{\pi D^*D^*} &= -g_{\pi D^*D^*}\epsilon^{\mu\nu\alpha\beta}\partial_\mu D^8_\nu\pi\partial_\alpha\bar{D}^*_\beta,\\
\mathcal{L}_{\rho DD^*} &= -g_{\rho DD^*}\epsilon^{\mu\nu\alpha\beta}(D\partial_\mu\rho_\nu\partial_\alpha\bar{D}^*_\beta + \partial_\mu D^*_\nu\partial_\alpha\rho_\beta\bar{D}).
\end{aligned} \tag{3}$$

In Eqs. (2) and (3), $D^{(*)}$ and $\bar{D}^{(*)}$ represent the isospin doublets of the pseudoscalar (vector) charmed mesons; ψ_ν denotes the $\psi(2S)$ vector field; $\vec{\tau}$ represents the Pauli matrices in the isospin space; $\vec{\pi}$ and $\vec{\rho}$ are the pion and ρ isospin triplets, respectively. The coupling constants $g_{\pi DD^*}$, $g_{\rho DD}$, $g_{\rho D^*D^*}$, $g_{\pi D^*D^*}$, and $g_{\rho DD^*}$ will be discussed below.

These effective Lagrangians introduced above allow us to determine the amplitudes of the $\psi(2S)$ absorption

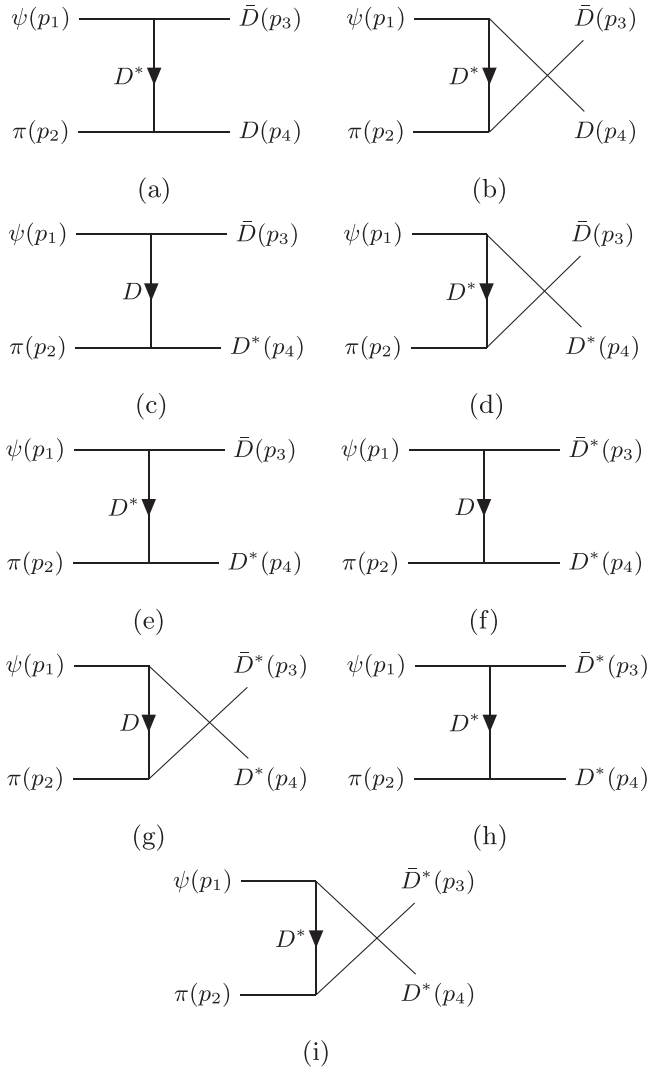

FIG. 1. Born diagrams for the processes $\psi(2S)\pi \to \bar{D}D$ [(a), (b)], $\psi(2S)\pi \to \bar{D}^*D$ [(c)–(e)], and $\psi(2S)\pi \to \bar{D}^*D^*$ [(f)–(i)]. The particle charges are not specified. We denote $\psi(2S) \equiv \psi$.

processes depicted in Figs. 1 and 2:

$$\begin{aligned}
\mathcal{M}_{\psi\pi\to\bar{D}D} &\equiv \sum_{i=a,b} \mathcal{M}^{(\mathbf{i})}, \\
\mathcal{M}_{\psi\pi\to\bar{D}D^*} &\equiv \sum_{\mathbf{i}=c,d,e} \mathcal{M}^{(\mathbf{i})}, \\
\mathcal{M}_{\psi\pi\to\bar{D}^*D^*} &\equiv \sum_{\mathbf{i}=f,g,h,i} \mathcal{M}^{(\mathbf{i})}, \\
\mathcal{M}_{\psi\rho\to\bar{D}D} &\equiv \sum_{\mathbf{i}=j,k,l,m} \mathcal{M}^{(\mathbf{i})}, \\
\mathcal{M}_{\psi\rho\to\bar{D}D^*} &\equiv \sum_{\mathbf{i}=n,o,p,q} \mathcal{M}^{(\mathbf{i})}, \\
\mathcal{M}_{\psi\rho\to\bar{D}^*D^*} &\equiv \sum_{\mathbf{i}=r,s,t,u} \mathcal{M}^{(\mathbf{i})},
\end{aligned} \tag{4}$$

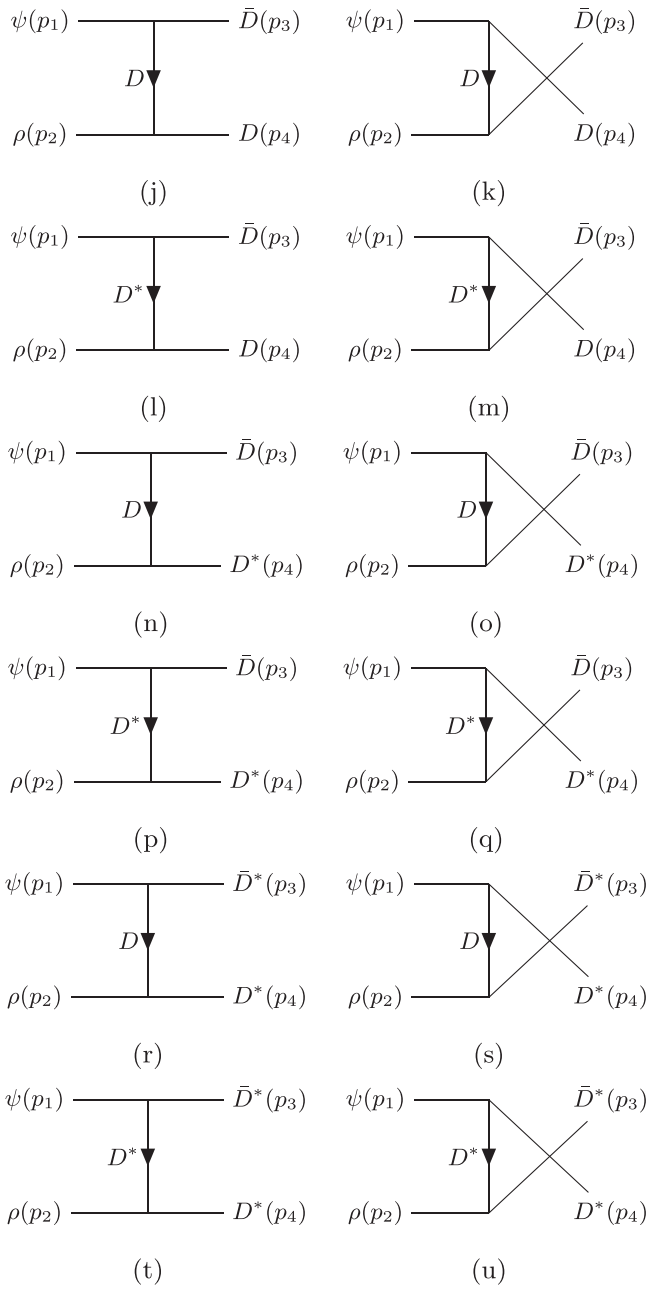

FIG. 2. Born diagrams for the processes $\psi(2S)\rho \to \bar{D}D$ [(j)–(m)], $\psi(2S)\rho \to \bar{D}^*D$ [(n)–(q)], and $\psi(2S)\rho \to \bar{D}^*D^*$ [(r)–(u)]. The particle charges are not specified. We denote $\psi(2S) \equiv \psi$.

where $\mathcal{M}^{(\mathbf{i})}$ denotes the contribution coming from the specific reaction (i); the expressions are explicitly summarized in the Appendix.

As usual, we employ form factors to prevent the artificial growth of the amplitudes with energy and take into account the finite size of hadrons. To the best of our knowledge, there is so far no systematic study of the couplings of Eqs. (2) and (3) involving $\psi(2S)$. Because of the similarities of these vertices with those involving J/ψ, we assume that the form factors for $\psi(2S)$ are given by the same

TABLE I. Form factors $g_{M_1M_2M_3}$ for the respective vertices $M_1M_2M_3$ presented in Eq. (5), computed via the QCD sum rules in Refs. [16,22,24–27] for J/ψ. M_2 denotes the exchanged particle.

$M_1\ M_2\ M_3$	Form	A	B	C
ψDD	II	5.8	20	15.8
ψD^*D	II	20	27	18.6
ψDD^*	II	13	26	21.2
ψD^*D^*	II	6.2	0	3.55
πDD^*	I	126	11.9	...
πD^*D	I	126	11.9	...
ρDD	I	37.5	12.1	...
ρD^*D^*	II	4.9	0	13.3
πD^*D^*	II	4.8	0	6.8
ρDD^*	I	234	44	...
ρD^*D	I	234	44	...

parametrizations of those for J/ψ, which have already been computed via QCD sum rules in Refs. [16,22,24–27]. They are given by

$$\text{(I)}\quad g_{M_1M_2M_3} = \frac{A}{Q^2+B},$$
$$\text{(II)}\quad g_{M_1M_2M_3} = Ae^{-\left(\frac{B+Q^2}{C}\right)}, \tag{5}$$

where Q is the Euclidean four-momentum of the off-shell particle involved in the vertex and the constants A, B, and C are given in Table I. The cross sections should depend on the size of the interacting hadron. From the studies of charmonium spectroscopy, it is well known that $\psi(2S)$ is larger than the fundamental charmonium state by a factor of about 2 (see, for example, the discussion in [28]). Therefore, based on geometrical arguments, we expect $\psi(2S)$ to have bigger cross sections than J/ψ by a factor of about 4. Hence, in the lack of reliable estimates of the coupling constants and form factors for the $\psi(2S)$ vertices, we use the parametrizations given in Eq. (5) and Table I but with the coupling constants varying in the range $[g_{M_1M_2M_3}, 2g_{M_1M_2M_3}]$. This will be the main source of uncertainties in our calculation.

III. CROSS SECTIONS FOR THE PROCESSES INVOLVING $\psi(2S)$

A. Vacuum cross sections

The isospin-spin-averaged cross section in the center-of-mass (c.m.) frame for a specific $ab \to cd$ process is given by

$$\sigma_{ab\to cd}(s) = \frac{1}{64\pi^2 s g_a g_b}\frac{|\vec{p}_{cd}|}{|\vec{p}_{ab}|}\int d\Omega \sum_{S,I}|\mathcal{M}_{ab\to cd}(s,\theta)|^2, \tag{6}$$

where $\sqrt{s}$ is the c.m. energy; $|\vec{p}_{ab}|$ and $|\vec{p}_{cd}|$ are the magnitudes of three-momenta of initial and final particles in the c.m. frame, respectively; $\sum_{S,I}$ means the sum over the spins and isospins of the particles in the initial and final state, weighted by the isospin and spin degeneracy factors $g_a = (2S_a+1)(2I_a+1)$ and $g_b = (2S_b+1)(2I_b+1)$ of the two particles forming the initial state.

It is worth remarking that the cross sections for the respective inverse processes can be computed through the use of the detailed balance relation:

$$\sigma_{cd\to ab}(s) = \frac{g_a g_b}{g_c g_d}\frac{|\vec{p}_{ab}|^2}{|\vec{p}_{cd}|^2}\sigma_{ab\to cd}. \tag{7}$$

The calculations are performed using the isospin-averaged masses of the light and heavy mesons according to the values reported by the PDG [1]. Since we use a range of values for the couplings involving $\psi(2S)$ due to the uncertainties, the results are shown in terms of bands.

The cross sections for the $\psi(2S)$ suppression by comoving light mesons as functions of the relative c.m. energy $\sqrt{s}-\sqrt{s_0}$ ($\sqrt{s_0}$ being the threshold energy of the respective channel) are plotted in Fig. 3. Except for the channels $\psi\pi \to \bar{D}^*D$ and $\psi\pi \to \bar{D}^*D^*$, all the cross sections are

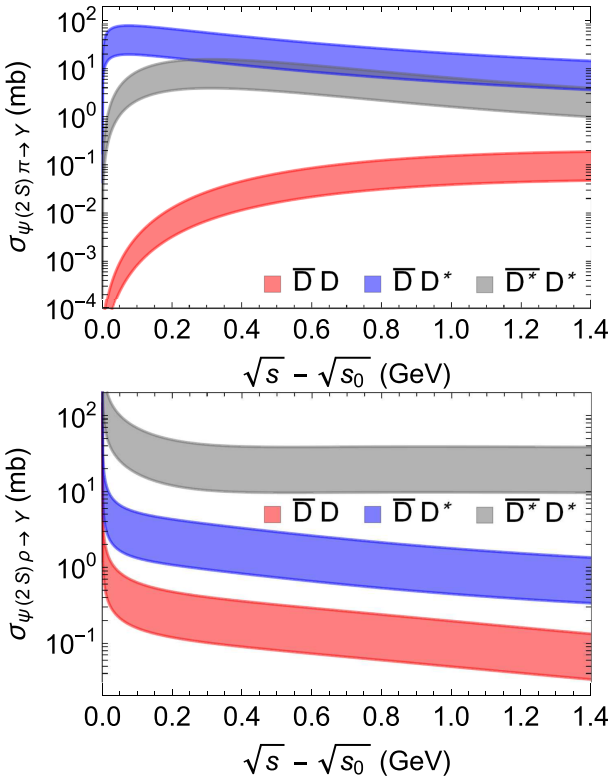

FIG. 3. Cross sections for the absorption processes $\psi\pi \to \bar{D}^{(*)}D^{(*)}$ (upper panel) and $\psi\rho \to \bar{D}^{(*)}D^{(*)}$ (lower panel), as functions of the relative c.m. energy $\sqrt{s}-\sqrt{s_0}$. $\sqrt{s_0}$ is the threshold energy of the respective channel.

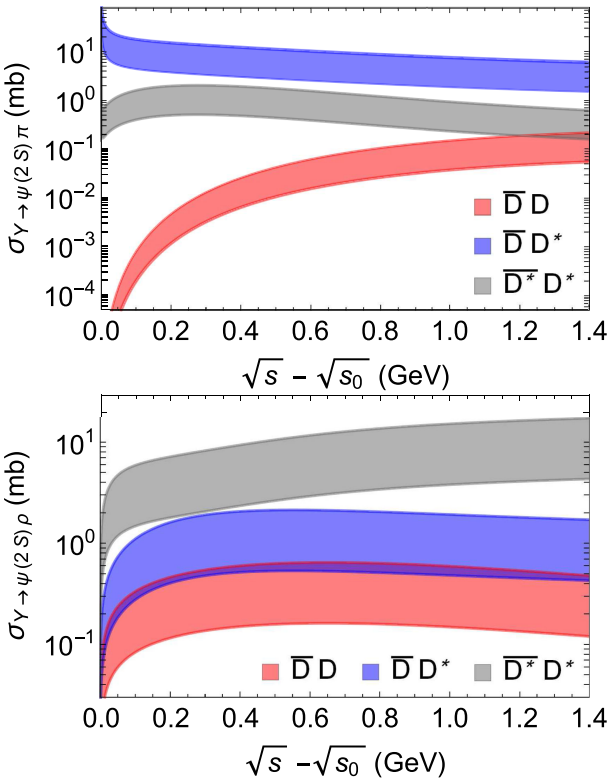

FIG. 4. Cross sections for the production processes $\bar{D}^{(*)}D^{(*)} \to \psi\pi$ (upper panel) and $\bar{D}^{(*)}D^{(*)} \to \psi\rho$ (lower panel), as functions of the relative c.m. energy $\sqrt{s} - \sqrt{s_0}$.

exothermic, showing a substantial decrease after the threshold. We remark that the $\psi\pi \to \bar{D}D$ channel acquires large cross sections close to the threshold, not visible in the plot, and after that it suffers a strong decrease. In the region close to the threshold up to moderate energies, i.e., $\sqrt{s} - \sqrt{s_0} \simeq 500$ MeV, the different channels present magnitudes of the order of $10^{-4} - 10^{1}$ mb, but with the reactions with final state $\bar{D}D$ being suppressed with respect to the other ones. In the case of the inverse processes, the cross sections are plotted in Fig. 4. As expected, very near the threshold, they have an opposite behavior with respect to the corresponding $\psi(2S)$-suppression reactions in Fig. 3. From the region close to the threshold up to moderate energies, we observe that the cross sections are of the order $10^{-4} - 10^{0}$ mb, and, in general, those for $\psi(2S)$-suppression reactions have smaller magnitudes than their respective inverse processes. This is an important feature (since it appears in the energy range relevant for heavy-ion collisions) which can be attributed to the differences in the phase space and the degeneracies encoded in Eq. (7) [17].

B. Thermally averaged cross sections

In a hadron gas, the temperature determines the order of magnitude of the collision energy. Hence, it is more realistic to use the vacuum cross sections weighted by the thermal momentum distributions of the colliding particles. For processes with a two-particle initial state going into two final state particles $ab \to cd$, it is given by [10,15–17,29]

$$\begin{aligned}\langle \sigma_{ab\to cd} v_{ab} \rangle &= \frac{\int d^3\mathbf{p}_a d^3\mathbf{p}_b f_a(\mathbf{p}_a) f_b(\mathbf{p}_b) \sigma_{ab\to cd} v_{ab}}{\int d^3\mathbf{p}_a d^3\mathbf{p}_b f_a(\mathbf{p}_a) f_b(\mathbf{p}_b)} \\ &= \frac{1}{4\beta_a^2 K_2(\beta_a)\beta_b^2 K_2(\beta_b)} \\ &\quad \times \int_{z_0}^{\infty} dz K_1(z) \sigma_{ab\to cd}(s = z^2 T^2) \\ &\quad \times [z^2 - (\beta_a + \beta_b)^2][z^2 - (\beta_a - \beta_b)^2], \end{aligned} \tag{8}$$

where v_{ab} denotes the relative velocity of the two initial interacting particles; the function $f_i(\mathbf{p}_i)$ is the Bose-Einstein distribution; $\beta_i = m_i/T$, with T being the temperature; $z_0 = \max(\beta_a + \beta_b, \beta_c + \beta_d)$, and K_1 and K_2 are the modified Bessel functions of the second kind. It can be seen from the expression in the second line in Eq. (8) that the thermal average suppresses the configurations very close to the thresholds: For sufficiently large z_0, the $K_1(z)$ function acquires very small values.

In Fig. 5, we plot the thermally averaged cross sections as functions of the temperature for the $\psi(2S)$ suppression by comoving light mesons using the vacuum cross-section

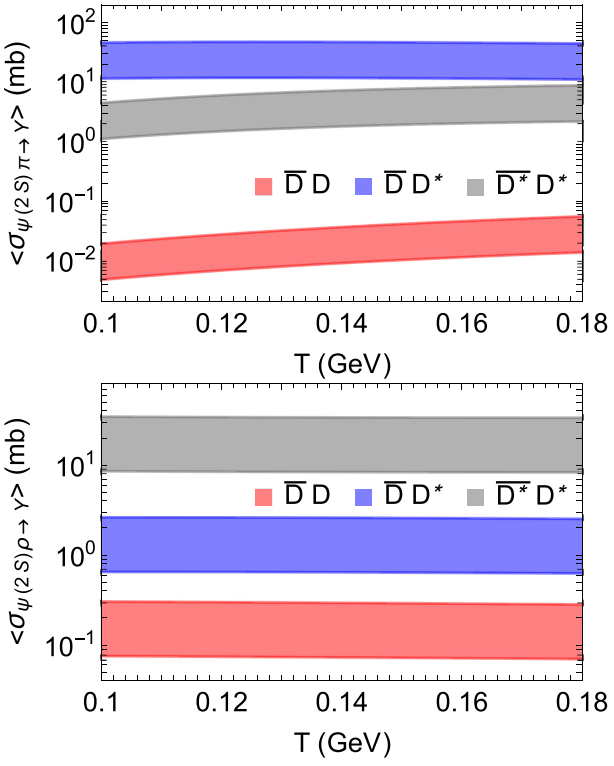

FIG. 5. Thermally averaged cross sections for the absorption processes $\psi\pi \to \bar{D}^{(*)}D^{(*)}$ (upper panel) and $\psi\rho \to \bar{D}^{(*)}D^{(*)}$ (lower panel), as functions of the temperature.

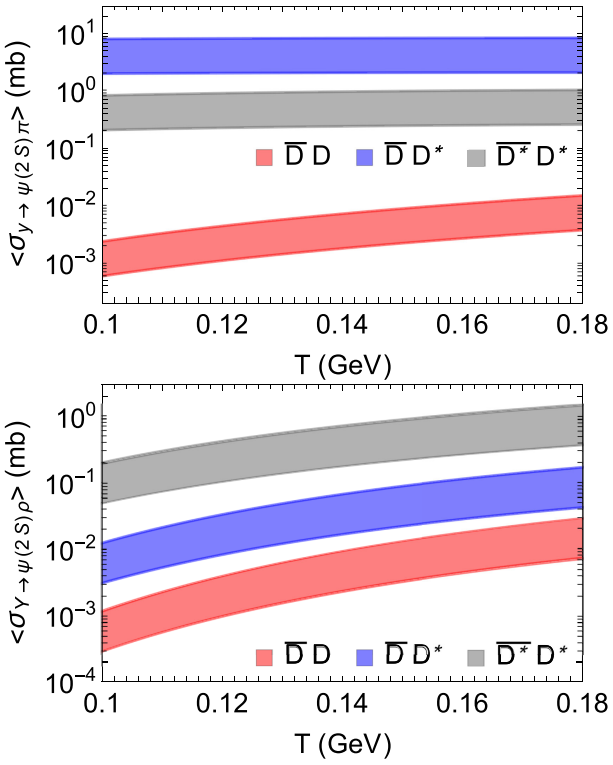

FIG. 6. Thermally averaged cross sections for the production processes $\bar{D}^{(*)}D^{(*)} \to \psi\pi$ (upper panel) and $\bar{D}^{(*)}D^{(*)} \to \psi\rho$ (lower panel), as functions of the temperature.

results obtained previously. In general, they have a weak dependence on the temperature. The tendency seen in the vacuum at moderate energies is reproduced here: Reactions with the $\bar{D}D$ final state are suppressed with respect to the other ones. On the other hand, for the $\psi(2S)$ production processes, shown in Fig. 6, the reactions involving the production of $\psi(2S)\rho$ present a strong dependence on the temperature. Most importantly, the absorption cross sections are always larger than the production ones, and the difference can reach 2 orders of magnitude, depending on the temperature. According to previous studies, this feature may have strong impact on the final yield of the $\psi(2S)$ in heavy-ion collisions. This issue will be addressed in the next section.

IV. MULTIPLICITIES OF $\psi(2S)$ AND $X(3872)$

A. Time evolution

Here, we will present the formalism used to determine the yields of $\psi(2S)$ and $X(3872)$ in a hadron gas formed in the final stage of heavy-ion collisions. We will use the thermally averaged cross sections estimated in the previous section for $\psi(2S)$. For $X(3872)$, we will use the results reported in Ref. [16] and include the contributions of the anomalous vertex $XD^{*}\bar{D}^{*}$ presented in Refs. [11,12]. These quantities will be employed as entries into the time-evolution equations to estimate the gain and loss terms. Explicitly, the rate equation is [10,12,16,20,23,30,31]

$$\frac{dN_h(\tau)}{d\tau} = \sum_{\substack{\bar{c}=\bar{D},\bar{D}^{*};\\ c=D,D^{*};\\ \varphi=\pi,\rho}} [\langle\sigma_{\bar{c}c\to\varphi h}v_{\bar{c}c}\rangle n_{\bar{c}}(\tau)N_c(\tau) - \langle\sigma_{\varphi h\to\bar{c}c}v_{\psi\varphi}\rangle n_{\varphi}(\tau)N_h(\tau)], \tag{9}$$

where $N_h(\tau)$ represents the multiplicity of the state of type h $[h = \psi(2S), X(3872)]$; $n_i(\tau)$ and $N_i(\tau)$ denote the density and the number of the meson of type i at a given τ, respectively. The pions, ρ, and charmed mesons in the reactions discussed previously are assumed to be in equilibrium, implying that with the Maxwell-Boltzmann approximation $n_i(\tau)$ becomes

$$n_i(\tau) \approx \frac{1}{2\pi^2}\gamma_i g_i m_i^2 T(\tau) K_2\left(\frac{m_i}{T(\tau)}\right), \tag{10}$$

where γ_i, g_i, and m_i are the fugacity, degeneracy factor, and particle mass i, respectively. The multiplicity $N_i(\tau)$ is then obtained by multiplying $n_i(\tau)$ by the volume $V(\tau)$. Following preceding works, we model the hadron gas expansion by the boost invariant Bjorken flow with an accelerated transverse expansion. The volume and temperature profiles as a function of the proper time τ are as follows [10,12,23,30,31]:

$$V(\tau) = \pi\left[R_C + v_C(\tau-\tau_C) + \frac{a_C}{2}(\tau-\tau_C)^2\right]^2 \tau c,$$
$$T(\tau) = T_C - (T_H - T_F)\left(\frac{\tau-\tau_H}{\tau_F-\tau_H}\right)^{\frac{4}{5}}, \tag{11}$$

where R_C, v_C, a_C, and T_C are the transverse size, transverse velocity, transverse acceleration, and temperature at the time τ_C, respectively; T_H (T_F) is the temperature at the hadronization (kinetic freeze-out) time τ_H (τ_F). The parameters in Eq. (11) are fixed according to Ref. [31] for a hadronic medium formed in central Pb-Pb collisions at $\sqrt{s_{NN}} = 5.02$ TeV; for completeness, they are given in Table II.

Additionally, the multiplicities of the light mesons as well as of the charm quarks in charmed mesons are also shown in Table II. For the light mesons, their fugacities in Eq. (10) appear as normalization parameters to adjust the multiplicities given in Table II. In the case of charm quarks, since they are produced in the early stages of the collision, we assume that the total number of charm quarks (N_c) in charmed hadrons remains approximately conserved during the hydrodynamic expansion, which leads to the condition $N_c = n_c(\tau) \times V(\tau) = \text{const}$, engendering a time-dependent charm-quark-fugacity factor $\gamma_c \equiv \gamma_c(\tau)$ in Eq. (10).

To fix the initial condition for the yield $N_h(\tau)$ appearing in the integro-differential equation (9), i.e., the yield of the

TABLE II. In the first three rows, we list the set of parameters used in Eq. (11) for the hydrodynamic expansion and cooling of the hadronic medium formed in central Pb-Pb collisions at $\sqrt{s_{NN}} = 5.02$ TeV [31]. In the fourth row, we list the multiplicity of the charm quark and light mesons used in the model. In the last two rows, the quark masses and the frequency used in the coalescence model are listed [16].

v_C (c)	a_C (c^2/fm)	R_C (fm)
0.5	0.09	11
τ_C (fm/c)	τ_H (fm/c)	τ_F (fm/c)
7.1	10.2	21.5
T_C (MeV)	T_H (MeV)	T_F (MeV)
156	156	115
N_c	$N_\pi(\tau_F)$	$N_\rho(\tau_H)$
14	2410	184
V_C (fm^3)	m_q (MeV)	m_c (MeV)
5380	350	1500
ω (MeV)		
220		

state h at the end of QGP, we employ the so-called coalescence model, which is characterized by the convolution of the density matrix of the constituents of h with its Wigner function [14,16,31]. This model has the advantage of carrying information on the intrinsic structure of the system, such as angular momentum and the type and number of constituent quarks. More concretely, according to this approach the yield of a hadronic state of type h can be written as

$$N_h \approx g_h \prod_{j=1}^{n} \frac{N_j}{g_j} \prod_{i=1}^{n-1} \frac{(4\pi\sigma_i^2)^{\frac{3}{2}}}{V(\tau)(1+2\mu_i T(\tau)\sigma_i^2)} \times \left[\frac{4\mu_i T(\tau)\sigma_i^2}{3(1+2\mu_i T(\tau)\sigma_i^2)}\right]^{l_i}, \tag{12}$$

where g_j and N_j are the degeneracy and number of the jth constituent of h and $\sigma_i = (\mu_i\omega)^{-1/2}$, respectively; the quantity ω is the oscillator frequency (taking an harmonic oscillator as a model of the hadron internal structure) and μ the reduced mass, i.e., $\mu^{-1} = m_{i+1}^{-1} + (\sum_{j=1}^{i} m_j)^{-1}$; l_i is the angular momentum of the system: It is 0 for an S wave and 1 for a P wave. Table II summarizes the oscillation frequency for the charmed hadrons, the charm quark number, and masses used here.

From Eq. (12), we have the following multiplicities for $\psi(2S)$ and $X(3872)$ at the end of the mixed phase:

$$\begin{aligned} N_{\psi(2S)}(\tau_H) &\approx 1.8 \times 10^{-4}, \\ N_X^{(4q)}(\tau_H) &\approx 1.8 \times 10^{-4}, \\ N_X^{(\mathrm{Mol})}(\tau_H) &\approx 1.1 \times 10^{-2}. \end{aligned} \tag{13}$$

In the case of the molecular state $X(3872)^{(\mathrm{Mol})}$, to calculate the oscillation frequency, we have employed the expression $\omega = 6B$, with B being the binding energy of $X(3872)$ considered as a $(D^0\bar{D}^{*0} + \mathrm{cc})$ bound state. As can be seen, the coalescence mechanism generates initial conditions in which molecules are more abundant than compact tetraquarks by a factor of about 60, reflecting the fact that forming a loosely bound state is easier than a compact tetraquark.

When compared to other works, the values for $N_X^{(4q)}(\tau_H)$ and $N_X^{(\mathrm{Mol})}(\tau_H)$ in Eq. (13) are somewhat smaller than the multiplicities reported in Ref. [30] because of the different values used for the parameters (e.g., N_c for the calculation of $N_X^{(4q)}$ and B for $N_X^{(\mathrm{Mol})}$). In addition, our value for $N_X^{(4q)}(\tau_H)$ in Eq. (13) is in agreement with that reported in Ref. [31]. However, $N_X^{(\mathrm{Mol})}(\tau_H)$ is bigger than the one in [31] by a factor of 2.4, again probably due to the different value used for B. Using a multiphase transport model, the authors of Ref. [32] obtained $N_X^{(4q)} \sim 2 \times 10^{-4}$ and $N_X^{(\mathrm{Mol})} \sim 4\text{–}5 \times 10^{-2}$ for more central Pb-Pb collisions at $\sqrt{s_{NN}} = 2.76$ TeV, which is of the same order of magnitude as our calculations.

In Fig. 7, we show the time evolution of the $\psi(2S)$ and $X(3872)$ multiplicities as a function of the proper time. In the case of $\psi(2S)$, the final yield increases by a factor of about one order of magnitude, which means that the gain terms in the evolution equation (9) play a dominant role at higher temperatures. Strictly speaking, at the beginning of the hadron gas phase, the densities and multiplicities of the charmed mesons are sufficient to counterbalance the bigger magnitudes of the thermal cross sections for the absorption processes multiplied by the densities of the light mesons and the multiplicity of $\psi(2S)$. As the time evolves, the gain and loss terms become almost of the same order (considering the uncertainties), and the $\psi(2S)$ multiplicity suffers just a slight reduction.

For the $X(3872)$ abundance, we remark that its time evolution has already been analyzed in Refs. [10,12] for central Au-Au collisions at $\sqrt{s_{NN}} = 200$ GeV. Very recently, in Ref. [16], this analysis has been redone for central Pb-Pb collisions at $\sqrt{s_{NN}} = 5.02$ TeV, for the purpose of comparison between the final yields of $T_{cc}^{+}(3985)$ and $X(3872)$. Since we are interested in the $X(3872)$ to $\psi(2S)$ yield ratio, for completeness we present again in Fig. 7 $N_{X(3872)}(\tau)$. This result is slightly different from that published in Ref. [16]. We improved the calculation including the anomalous vertex $XD^*\bar{D}^*$ as discussed in [11]. As can be seen from the figure, tetraquarks reach a final yield which is much smaller (by a factor of about 50) than the one of $(D\bar{D}^* + \mathrm{cc})$ molecules. Another feature is that in both cases the $X(3872)$ abundance does not present a sizable change with time.

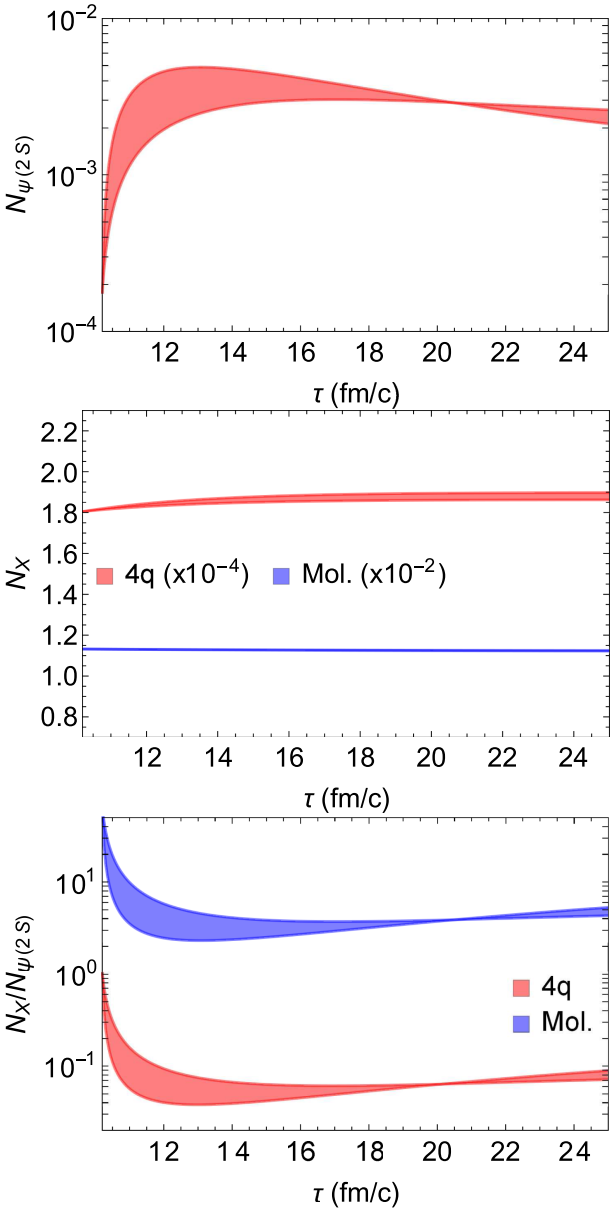

FIG. 7. Multiplicity of $\psi(2S)$ (upper panel), $X(3872)$ (central panel), and their ratio (lower panel) as a function of the proper time in central Pb-Pb collisions at $\sqrt{s_{NN}} = 5.02$ TeV.

We also show in Fig. 7 the time evolution of the $X(3872)$ to $\psi(2S)$ yield ratio. As expected from the discussion above, we observe a strong variation of this ratio in the early times and after that a relative stabilization. Interestingly, the molecular configuration generates a ratio greater than 1, which seems compatible with the value given in Eq. (1) obtained by the CMS Collaboration for Pb-Pb collisions at $\sqrt{s_{NN}} = 5.02$ TeV within the rapidity and transverse momentum ranges $|y| < 1.6$ and $15 < p_T < 50$ GeV. Since the data have been collected at high-transverse momenta and in a specific rapidity range, whereas our results have been computed considering the whole range in p_T and y, a direct comparison between our results and data is not possible yet. It should be mentioned that in Ref. [9] the coalescence model has been used to estimate the N_X and the statistical hadronization model to obtain $N_{\Psi(2S)}$. However, the hadronic interactions have not been taken into account. This has resulted in a ratio with a central value of 0.806 for $X(3872)$ in the molecular configuration, argued to be consistent with the observed one. As shown in Fig. 7, we find a bigger ratio for the molecular configuration than that in Ref. [9].

B. Source size dependence

The size of the source can be related to a measurable quantity, the charged-particle pseudorapidity density at midrapidity, $dN_{ch}/d\eta(|\eta| < 0.5)$, which, in turn, can be related to the freeze-out temperature by means of the empirical formula [16,19,33]:

$$T_F = T_{F0} e^{-b\mathcal{N}}, \tag{14}$$

where $T_{F0} = 132.5$ MeV, $b = 0.02$, and $\mathcal{N} \equiv [dN_{ch}/d\eta(|\eta| < 0.5)]^{1/3}$. Assuming that the hadron gas undergoes a Bjorken cooling, i.e., $T = T_h(\tau_h/\tau)^{1/3}$, then the freeze-out time τ_F can be written in terms of $\mathcal{N}$ as [16,19,33]

$$\tau_F = \tau_H \left(\frac{T_H}{T_{F0}}\right)^3 e^{3b\mathcal{N}}. \tag{15}$$

A larger source generates a bigger $\mathcal{N}$, which, from the equation above, implies a bigger τ_F, i.e., a longer hadron gas phase. As a consequence, the use of Eq. (15) in (9) will give rise to a dependence of the multiplicity N_h on the size of the source.

As shown in Ref. [19], empirical formulas relating $\mathcal{N}$ with the volume of the system (V), charm quark number (N_c), and light quark number (N_q) can also be obtained. They are

$$\begin{aligned} V &= 2.82\mathcal{N}^3, \\ N_c &= 7.9 \times 10^{-5}\mathcal{N}^{4.8}, \\ N_u &= N_d = 0.37\mathcal{N}^3. \end{aligned} \tag{16}$$

We also assume that the charm quark number and the number of D mesons (N_D) are proportional. Hence, the use of Eq. (16) in (13) to estimate the dependence of the initial conditions with $\mathcal{N}$, together with (15) in (9), generates a dependence of N_h on $\mathcal{N}$.

In Fig. 8, we observe that the ratio $\mathcal{R}$ grows with $\mathcal{N}$. This is in qualitative agreement with the existing data. As mentioned in introduction, the LHCb Collaboration reported in Ref. [8] the growth of the ratio $\mathcal{R}$ when we go from pp to p-Pb and to Pb-Pb collisions. Our results give qualitative support to the conjecture that $X(3872)$ and

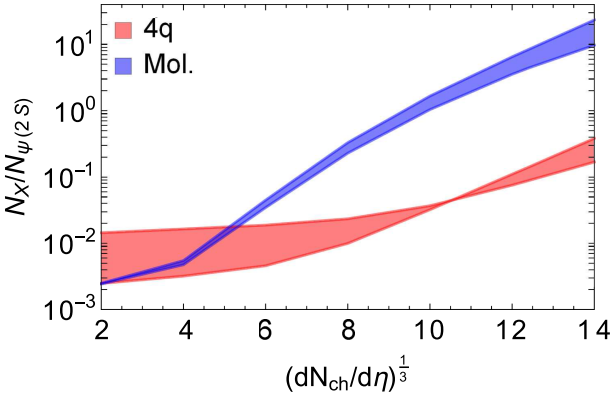

FIG. 8. Ratio $\mathcal{R}$ as a function of $\mathcal{N}$.

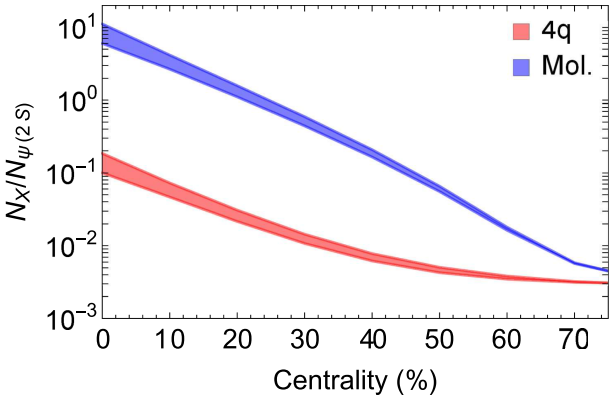

FIG. 9. The ratio $\mathcal{R}$ as a function of centrality in Pb-Pb collisions at $\sqrt{s_{NN}} = 5.02$ TeV.

$\psi(2S)$ experience a different dynamics in the hadronic medium. Unfortunately, a direct comparison is an involved task, as the data in Ref. [8] for the pp, p-Pb, and Pb-Pb (this last one from the CMS Collaboration) collisions refer to different energies and ranges of rapidity and transverse momentum. Interestingly, the curves of the molecular and compact tetraquark configurations converge to each other at smaller sources, but in the region of validity of this model (larger sources) the difference between these configurations remains approximately of the same order.

C. Centrality and energy dependence

Apart from its dependence on the mass number A, $\mathcal{N}$ also depends on the centrality of the collision and on the center-of-mass collision energy ($\sqrt{s}$). For Pb-Pb collisions at 5.02 TeV, the relation between $\mathcal{N}$ and the centrality (denoted as x, in percent) can be parametrized as [19]

$$\left.\frac{dN_{ch}}{d\eta}\right|_{|\eta|<0.5} = 2142.16 - 85.76x + 1.89x^2 - 0.03x^3 + 3.67\times10^{-5}x^4 - 2.24\times10^{-6}x^5 + 5.25\times10^{-9}x^6. \quad (17)$$

Similarly, the dependence of $\mathcal{N}$ on $\sqrt{s}$ can be parametrized as

$$\left.\frac{dN_{ch}}{d\eta}\right|_{|\eta|<0.5} = -2332.12 + 491.69\log(220.06+\sqrt{s}). \quad (18)$$

In order to determine the initial $\psi(2S)$ and $X(3872)$ multiplicities with the coalescence model in terms of the centrality and of $\sqrt{s}$, we insert Eqs. (17) and (18) into Eq. (16) and use these new equations in Eq. (12). The final yields are then obtained solving Eq. (9) with these initial conditions and up to a final time τ_F (which is also $\mathcal{N}$ dependent).

In Fig. 9, we show the ratio $\mathcal{R}$ as a function of the centrality. The $X(3872)$ final yield decreases faster than the one of $\psi(2S)$ as we move from central to peripheral collisions, and, therefore, the ratio becomes smaller. Also, the curves for the molecular and compact tetraquark configurations converge to similar values for more peripheral collisions.

The ratio $\mathcal{R}$ as a function of the energy $\sqrt{s}$ in central Pb-Pb collisions is shown in Fig. 10. The $X(3872)$ final yield presents an enhancement compared to that of $\psi(2S)$, resulting in a bigger ratio as $\sqrt{s}$ increases; the difference between the curves of the molecular and compact tetraquark configurations remains of the same order at different energies.

Taking together the results in Figs. 7–10, we conclude that in central Pb-Pb collisions at $\sqrt{sNN} = 5.02$ TeV the ratio $\mathcal{R}$ for minimum bias events is

$$\frac{N_X}{N_{\psi(2S)}} \simeq 5 \quad \text{for molecules,}$$
$$\frac{N_X}{N_{\psi(2S)}} \simeq 0.1 \quad \text{for tetraquarks.} \quad (19)$$

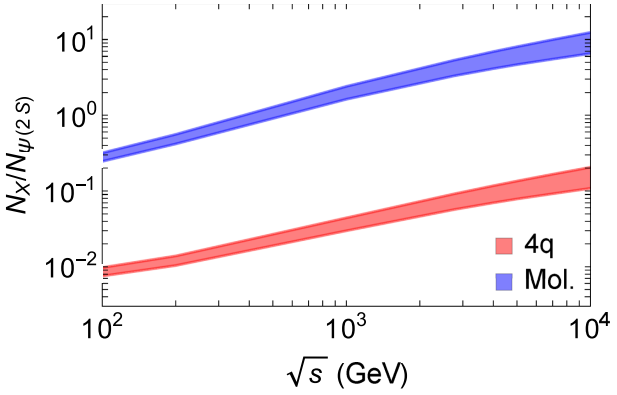

FIG. 10. The ratio $\mathcal{R}$ as a function of energy $\sqrt{s}$ in central Pb-Pb collisions.

This is the main result of our work, and it is our prediction for future measurements at run 3 of the ALICE Collaboration, where it will be possible to measure $X(3872)$ and $\psi(2S)$ at low transverse momentum, i.e., $2 < p_T < 8$ GeV, where the hydrodynamical approach used in this work should be applicable, as well as one can expect most of the yields of the mentioned states (see, for example, the transverse momentum distributions calculated in Refs. [9,34]). With data taken in this p_T range, it will be possible, for the first time, to investigate the medium effects on $X(3872)$, on $\psi(2S)$, and on their ratio and check our predictions. Moreover, in view of the numbers above, we may have a good chance to discriminate between molecules and tetraquarks. From the figures, we also conclude that is easier to identify the different configurations in larger systems and in more central collisions. Changing the collision energy is not so relevant for this purpose.

Before closing this section, we mention the study presented in Ref. [35], where the authors study the effects of a partonic medium on the ratio $\mathcal{R}$. They find a nontrivial behavior of this ratio. However, they do not consider final state hadronic interactions, as we do here. A combination of both approaches seems to be a promising project.

V. CONCLUDING REMARKS

In this work, we have studied the $X(3872)$ to $\psi(2S)$ yield ratio in heavy-ion collisions, taking into account the interactions of the $\psi(2S)$ and $X(3872)$ states with a hadron gas made of light mesons. To this end, the thermally averaged cross sections for the production and absorption of the $\psi(2S)$ have been evaluated for the first time by using effective Lagrangians. These cross sections, together with the thermally averaged cross sections for the $X(3872)$ production and absorption analyzed in previous works, have been employed in the rate equation to determine the time evolution of $N_{\psi(2S)}$, N_X, and $N_X/N_{\psi(2S)}$. The coalescence model has been used to compute the initial multiplicities, with $X(3872)$ being treated both as a molecular bound state and as a compact tetraquark. Our results indicate that the ratio is strongly affected by the combined effects of hadronic interactions and hydrodynamical expansion, and the molecular configuration has a final value bigger than one, while the compact tetraquark gives a smaller ratio by a factor of about 50.

Other interesting finding is that the ratio $\mathcal{R}$ grows with the size of the source, which is in qualitative agreement with the data from LHCb and CMS Collaborations [8].

We believe that this study can be seen as a theoretical support to the idea that $X(3872)$ and conventional charmonium $\psi(2S)$ have a different dynamics in a hadronic medium.

ACKNOWLEDGMENTS

This work was supported by the Brazilian agencies CNPq, Fundacao de Amparo a Pesquisa do Estado de Sao Paulo (FAPESP), and Conselho Nacional de Pesquisas Cientificas (CNPq)/Fundacao de Amparo a Pesquisa do Estado do Rio de Janeiro (FAPERJ) (Project INCT-Física Nuclear e Aplicações, Contract No. 464898/2014-5). The authors are deeply grateful to R. Rapp, who encouraged us to study this subject and with whom we had so many fruitful discussions. We thank Su-Houng Lee and Marcelo Munhoz for useful discussions.

APPENDIX: AMPLITUDES

Here, the expressions for the contributions to the amplitudes in Eq. (4), associated to the reactions depicted in Figs. 1 and 2, are given:

$$\mathcal{M}^{(a)} = g_{\psi DD^*} g_{\pi DD^*} \varepsilon_1^\mu \frac{1}{t - -m_{D^*}^2} \epsilon_{\mu\beta\lambda\rho} \left(-g^{\alpha\beta} + \frac{(p_1 - -p_3)^\alpha (p_1 - -p_3)^\beta}{m_{D^*}^2} \right) p_{2\alpha} p_1^\lambda p_3^\rho, \tag{A1}$$

$$\mathcal{M}^{(b)} = g_{\psi DD^*} g_{\pi DD^*} \varepsilon_1^\mu \frac{1}{u - -m_{D^*}^2} \epsilon_{\mu\beta\lambda\rho} \left(-g^{\alpha\beta} + \frac{(p_1 - -p_4)^\alpha (p_1 - -p_4)^\beta}{m_{D^*}^2} \right) p_{2\alpha} p_1^\lambda p_4^\rho, \tag{A2}$$

$$\mathcal{M}^{(c)} = 2 g_{\psi DD} g_{\pi DD^*} \varepsilon_1^\mu \varepsilon_4^{*\nu} \frac{1}{t - -m_D^2} p_{2\nu} p_{3\mu},$$

$$\mathcal{M}^{(d)} = \frac{1}{2} g_{\psi D^* D^*} g_{\pi DD^*} \varepsilon_1^\mu \varepsilon_4^{*\nu} \frac{1}{u - -m_{D^*}^2} \left(-g^{\alpha\beta} + \frac{(p_1 - -p_4)^\alpha (p_1 - -p_4)^\beta}{m_{D^*}^2} \right) (p_2 + p_3)_\alpha \times [2 p_{4\mu} g_{\nu\beta} - (p_1 + p_4)_\beta g_{\mu\nu} + 2 p_{1\nu} g_{\mu\beta}], \tag{A3}$$

$$\mathcal{M}^{(e)} = g_{\psi DD^*} g_{\pi D^* D^*} \varepsilon_1^\mu \varepsilon_4^{*\nu} \frac{1}{t - -m_{D^*}^2} \epsilon_{\mu\gamma\delta\beta} \epsilon_{\nu\lambda\rho\alpha} \left(-g^{\alpha\beta} + \frac{(p_1 - -p_3)^\alpha (p_1 - -p_3)^\beta}{m_{D^*}^2} \right) p^\gamma p_2^\rho p_3^\delta p_4^\lambda, \tag{A4}$$

$$\mathcal{M}^{(f)} = g_{\psi DD^*} g_{\pi DD^*} \varepsilon_1^{\mu} \varepsilon_3^{*\lambda} \varepsilon_4^{*\nu} \frac{1}{t - -m_D^2} \epsilon_{\mu\lambda\gamma\delta} p_1^{\gamma} p_{2\nu} p_3^{\delta},$$

$$\mathcal{M}^{(g)} = -g_{\psi DD^*} g_{\pi DD^*} \varepsilon_1^{\mu} \varepsilon_3^{*\lambda} \varepsilon_4^{*\nu} \frac{1}{u - -m_D^2} \epsilon_{\mu\nu\gamma\delta} p_1^{\gamma} p_{2\lambda} p_4^{\delta},$$

$$\mathcal{M}^{(h)} = g_{\psi D^* D^*} g_{\pi D^* D^*} \varepsilon_1^{\mu} \varepsilon_3^{*\lambda} \varepsilon_4^{*\nu} \frac{1}{t - -m_{D^*}^2} \epsilon_{\nu\gamma\delta\alpha} \left(-g^{\alpha\beta} + \frac{(p_1 - -p_3)^{\alpha} (p_1 - -p_3)^{\beta}}{m_{D^*}^2} \right) p_4^{\gamma} p_2^{\delta} \times [2p_{3\mu} g_{\beta\lambda} - -(p_1 + p_3)_{\beta} g_{\mu\lambda} + 2p_{1\lambda} g_{\mu\beta}], \tag{A5}$$

$$\mathcal{M}^{(i)} = g_{\psi D^* D^*} g_{\pi D^* D^*} \varepsilon_1^{\mu} \varepsilon_3^{*\lambda} \varepsilon_4^{*\nu} \frac{1}{u - -m_{D^*}^2} \epsilon_{\lambda\gamma\delta\alpha} \left(-g^{\alpha\beta} + \frac{(p_1 - -p_4)^{\alpha} (p_1 - -p_4)^{\beta}}{m_{D^*}^2} \right) p_2^{\gamma} p_3^{\delta} \times [2p_{4\mu} g_{\beta\nu} - -(p_1 + p_4)_{\beta} g_{\mu\nu} + 2p_{1nu} g_{\mu\beta}], \tag{A6}$$

$$\mathcal{M}^{(j)} = 4 g_{\psi DD} g_{\rho DD} \varepsilon_1^{\mu} \varepsilon_2^{\nu} \frac{1}{t - -m_D^2} p_{3\mu} p_{4\nu},$$

$$\mathcal{M}^{(k)} = 4 g_{\psi DD} g_{\rho DD} \varepsilon_1^{\mu} \varepsilon_2^{\nu} \frac{1}{u - -m_D^2} p_{3\nu} p_{4\mu},$$

$$\mathcal{M}^{(l)} = g_{\psi DD^*} g_{\rho DD^*} \varepsilon_1^{\mu} \varepsilon_2^{\nu} \frac{1}{t - -m_{D^*}^2} \epsilon_{\nu\gamma\delta\alpha} \epsilon_{\mu\lambda\rho\beta} \left(- - g^{\alpha\beta} + \frac{(p_1 - -p_3)^{\alpha} (p_1 - -p_3)^{\beta}}{m_{D^*}^2} \right) p_1^{\lambda} p_2^{\gamma} p_3^{\rho} p_4^{\delta}, \tag{A7}$$

$$\mathcal{M}^{(m)} = -g_{\psi DD^*} g_{\rho DD^*} \varepsilon_1^{\mu} \varepsilon_2^{\nu} \frac{1}{u - -m_{D^*}^2} \epsilon_{\nu\gamma\delta\alpha} \epsilon_{\mu\lambda\rho\beta} \left(- - g^{\alpha\beta} + \frac{(p_1 - -p_4)^{\alpha} (p_1 - -p_4)^{\beta}}{m_{D^*}^2} \right) p_1^{\lambda} p_2^{\delta} p_3^{\gamma} p_4^{\rho}, \tag{A8}$$

$$\mathcal{M}^{(n)} = -2 g_{\psi DD} g_{\rho DD^*} \varepsilon_1^{\mu} \varepsilon_2^{\nu} \varepsilon_4^{*\lambda} \frac{1}{t - -m_D^2} \epsilon_{\nu\lambda\gamma\delta} p_2^{\delta} p_4^{\gamma} p_{3\mu},$$

$$\mathcal{M}^{(o)} = 2 g_{\psi DD} g_{\rho DD^*} \varepsilon_1^{\mu} \varepsilon_2^{\nu} \varepsilon_4^{*\lambda} \frac{1}{u - -m_D^2} \epsilon_{\lambda\mu\gamma\delta} p_1^{\gamma} p_4^{\delta} p_{3\nu},$$

$$\mathcal{M}^{(p)} = g_{\psi DD^*} g_{\rho D^* D^*} \varepsilon_1^{\mu} \varepsilon_2^{\nu} \varepsilon_4^{*\lambda} \frac{1}{t - -m_{D^*}^2} \epsilon_{\mu\gamma\delta\beta} \left(-g^{\alpha\beta} + \frac{(p_1 - p_3)^{\alpha} (p_1 - 3)^{\beta}}{m_{D^*}^2} \right) p_1^{\gamma} p_3^{\delta} \times [2p_{4\nu} g_{\lambda\alpha} - -(p_2 + p_4)_{\alpha} g_{\nu\lambda} + 2p_{2\lambda} g_{\nu\alpha}], \tag{A9}$$

$$\mathcal{M}^{(q)} = g_{\psi D^* D^*} g_{\rho DD^*} \varepsilon_1^{\mu} \varepsilon_2^{\nu} \varepsilon_4^{*\lambda} \frac{1}{u - -m_{D^*}^2} \epsilon_{\nu\gamma\delta\beta} \left(- - g^{\alpha\beta} + \frac{(p_1 - -p_4)^{\alpha} (p_1 - -p_4)^{\beta}}{m_{D^*}^2} \right) p_2^{\delta} p_3^{\gamma} \times [2p_{4\mu} g_{\beta\lambda} - -(p_1 + p_4)_{\beta} g_{\mu\lambda} + 2p_{1\lambda} g_{\mu\beta}], \tag{A10}$$

$$\mathcal{M}^{(r)} = -g_{\psi DD^*} g_{\rho DD^*} \varepsilon_1^{\mu} \varepsilon_2^{\nu} \varepsilon_3^{*\rho} \varepsilon_4^{*\lambda} \frac{1}{t - -m_D^2} \epsilon_{\nu\lambda\gamma\delta} \epsilon_{\mu\rho\alpha\beta} p_1^{\alpha} p_2^{\delta} p_3^{\delta} p_4^{\gamma}, \tag{A11}$$

$$\mathcal{M}^{(s)} = g_{\psi DD^*} g_{\rho DD^*} \varepsilon_1^{\mu} \varepsilon_2^{\nu} \varepsilon_3^{*\rho} \varepsilon_4^{*\lambda} \frac{1}{u - -m_D^2} \epsilon_{\nu\rho\gamma\delta} \epsilon_{\mu\lambda\alpha\beta} p_1^{\alpha} p_2^{\gamma} p_3^{\delta} p_4^{\beta}, \tag{A12}$$

$$\mathcal{M}^{(t)} = g_{\psi D^* D^*} g_{\rho D^* D^*} \varepsilon_1^{\mu} \varepsilon_2^{\nu} \varepsilon_3^{*\rho} \varepsilon_4^{*\lambda} \frac{1}{t - -m_{D^*}^2} \left(-g^{\alpha\beta} + \frac{(p_1 - -p_3)^{\alpha} (p_1 - -p_3)^{\beta}}{m_{D^*}^2} \right) \times [2p_{4\nu} g_{\alpha\lambda} - -(p_2 + p_4)_{\alpha} g_{\nu\lambda} + 2p_{2\lambda} g_{\nu\alpha}][2p_{3\mu} g_{\beta\rho} - -(p_1 + p_3)_{\beta} g_{\mu\rho} + 2p_{1\rho} g_{\mu\beta}], \tag{A13}$$

$$\mathcal{M}^{(u)} = g_{\psi D^* D^*} g_{\rho D^* D^*} \varepsilon_1^{\mu} \varepsilon_2^{\nu} \varepsilon_3^{*\rho} \varepsilon_4^{*\lambda} \frac{1}{u - -m_{D^*}^2} \left(-g^{\alpha\beta} + \frac{(p_1 - -p_4)^{\alpha} (p_1 - -p_4)^{\beta}}{m_{D^*}^2} \right)$$
$$\times [2p_{3\nu} g_{\alpha\rho} - -(p_2 + p_3)_{\alpha} g_{\nu\rho} + 2p_{2\rho} g_{\nu\alpha}][2p_{4\mu} g_{\beta\lambda} - -(p_1 + p_4)_{\beta} g_{\mu\lambda} + 2p_{1\lambda} g_{\mu\beta}], \tag{A14}$$

where p_1 and p_2 are the momenta of initial state particles while p_3 and p_4 are those of final state particles; s, t, and u are the Mandelstam variables: $s = (p_1 + p_2)^2$, $t = (p_1 - p_3)^2$, and $u = (p_1 - p_4)^2$; and $\epsilon_{\mathbf{i}}^{(*)} \equiv \epsilon^{(*)}(p_i)$ is the polarization vector.

[1] R. L. Workman *et al.* (Particle Data Group), Prog. Theor. Exp. Phys. **2022**, 083C01 (2022).
[2] C. Z. Yuan, EPJ Web Conf. **274**, 01001 (2022).
[3] N. Brambilla, S. Eidelman, C. Hanhart, A. Nefediev, C. P. Shen, C. E. Thomas, A. Vairo, and C. Z. Yuan, Phys. Rep. **873**, 1 (2020); S. Narison, F. S. Navarra, and M. Nielsen, Phys. Rev. D **83**, 016004 (2011).
[4] H. X. Chen, W. Chen, X. Liu, Y. R. Liu, and S. L. Zhu, Rep. Prog. Phys. **86**, 026201 (2023).
[5] S. K. Choi *et al.* (Belle Collaboration), Phys. Rev. Lett. **91**, 262001 (2003).
[6] A. M. Sirunyan *et al.* (CMS Collaboration), Phys. Rev. Lett. **128**, 032001 (2022).
[7] R. Aaij *et al.* (LHCb Collaboration), Phys. Rev. Lett. **126**, 092001 (2021).
[8] R. Aaij *et al.* (LHCb Collaboration), arXiv:2402.14975.
[9] H. Yun, D. Park, S. Noh, A. Park, W. Park, S. Cho, J. Hong, Y. Kim, S. Lim, and S. H. Lee, Phys. Rev. C **107**, 014906 (2023).
[10] S. Cho and S. H. Lee, Phys. Rev. C **88**, 054901 (2013).
[11] A. M. Torres, K. P. Khemchandani, F. S. Navarra, M. Nielsen, and L. M. Abreu, Phys. Rev. D **90**, 114023 (2014).
[12] L. M. Abreu, K. P. Khemchandani, A. Martinez Torres, F. S. Navarra, and M. Nielsen, Phys. Lett. B **761**, 303 (2016).
[13] L. M. Abreu, F. S. Navarra, and M. Nielsen, Phys. Rev. C **101**, 014906 (2020).
[14] L. M. Abreu, Phys. Rev. D **103**, 036013 (2021).
[15] L. M. Abreu, F. S. Navarra, M. Nielsen, and H. P. L. Vieira, Eur. Phys. J. C **82**, 296 (2022).
[16] L. M. Abreu, H. P. L. Vieira, and F. S. Navarra, Phys. Rev. D **105**, 116029 (2022).
[17] L. M. Abreu, F. S. Navarra, and H. P. L. Vieira, Phys. Rev. D **106**, 076001 (2022).
[18] L. M. Abreu, F. S. Navarra, and H. P. L. Vieira, Phys. Rev. D **106**, 074028 (2022).
[19] L. M. Abreu, F. S. Navarra, M. Nielsen, and H. P. L. Vieira, Phys. Rev. D **107**, 114013 (2023).
[20] L. M. Abreu, R. O. Magalhães, F. S. Navarra, and H. P. L. Vieira, arXiv:2310.18747.
[21] Yongseok Oh, Taesoo Song, and Su Houng Lee, Phys. Rev. C **63**, 034901 (2001).
[22] F. Carvalho, F. O. Durães, F. S. Navarra, and M. Nielsen, Phys. Rev. C **72**, 024902 (2005).
[23] L. M. Abreu, K. P. Khemchandani, A. Martínez Torres, F. S. Navarra, and M. Nielsen, Phys. Rev. C **97**, 044902 (2018).
[24] J. Lu, G. L. Yu, and Z. G. Wang, Eur. Phys. J. A **59**, 195 (2023).
[25] M. E. Bracco, M. Chiapparini, F. S. Navarra, and M. Nielsen, Prog. Part. Nucl. Phys. **67**, 1019 (2012).
[26] M. E. Bracco, M. Chiapparini, F. S. Navarra, and M. Nielsen, Phys. Lett. B **659**, 559 (2008).
[27] B. O. Rodrigues, M. E. Bracco, M. Nielsen, and F. S. Navarra, Nucl. Phys. **A852**, 127 (2011).
[28] S. Godfrey and N. Isgur, Phys. Rev. D **32**, 189 (1985).
[29] P. Koch and B. Muller, J. Rafelski. Phys. Rep. **142**, 167 (1986).
[30] S. Cho, T. Furumoto, T. Hyodo, D. Jido, C. M. Ko, S. H. Lee, M. Nielsen, A. Ohnishi, T. Sekihara, S. Yasui, and K. Yazaki (ExHIC Collaboration), Phys. Rev. Lett. **106**, 212001 (2011).
[31] S. Cho *et al.* (EXHIC Collaboration), Prog. Part. Nucl. Phys. **95**, 279 (2017).
[32] H. Zhang, J. Liao, E. Wang, Q. Wang, and H. Xing, Phys. Rev. Lett. **126**, 012301 (2021).
[33] C. Le Roux, F. S. Navarra, and L. M. Abreu, Phys. Lett. B **817**, 136284 (2021).
[34] A. Andronic, P. Braun-Munzinger, M. K. Köhler, K. Redlich, and J. Stachel, Phys. Lett. B **797**, 134836 (2019).
[35] Y. Guo, X. Guo, J. Liao, E. Wang, and H. Xing, arXiv:2302.03828.